Structural Engineering and Mechanics, Vol. 18, No. 5 (2004) 627-644

DOI: http://dx.doi.org/10.12989/sem.2004.18.5.627

Endochronic simulation for viscoplastic collapse of long, thick-walled tubes subjected to external pressure and axial tension

Kuo-Long Lee†

Department of Mechanical Engineering, Far East College, Tainan, Taiwan, R.O.C.

Kao-Hua Chang‡

Department of Engineering Science, National Cheng Kung University, Tainan, Taiwan, R.O.C.

(Received November 7, 2003, Accepted June 4, 2004)

Abstract. In this study, the endochronic theory was used to investigate the collapse of thick-walled tubes subjected to external pressure and axial tension. The experimental and theoretical findings of Madhavan *et al.* (1993) for thick-walled tubes of 304 stainless steel subjected to external pressure and axial tension were compared with the endochronic simulation. Collapse envelopes for various diameter-to-thickness tubes under two different pressure-tension loadings were involved. It has been shown that the experimental results were aptly described by the endochronic approach demonstrated from comparison with the theoretical prediction employed by Madhavan *et al.* (1993). Furthermore, by using the rate-sensitivity function of the intrinsic time measure proposed by Pan and Chern (1997) in the endochronic theory, our theoretical analysis was extended to investigate the viscoplastic collapse of thick-walled tubes subjected to external pressure and axial tension. It was found that the pressure-tension collapse envelopes are strongly influenced by the strain-rate during axial tension. Due to the hardening of the metal tube of 304 stainless steel under a faster strain-rate during uniaxial tension, the size of the tension-collapse envelope increases.

Key words: endochronic theory; viscoplastic collapse; thick-walled tubes, external pressure and axial tension.

1. Introduction

Long, thick-walled tubes are widely used for many practical applications, such as offshore pipelines, offshore deep-water platforms, and tubular components in nuclear reactors. In various applications, long, thick-walled tubes are constantly subjected to diverse loading conditions, such as external pressure, bending, or axial tension. Due to advancements in experimental facilities, complicated loading histories for long, thick-walled tubes can be performed in the laboratory.

† Assistant Professor
‡ Graduate Student

However, a theoretical approach must not only be simulated the experimental result, but can be extended to predict the possible behaviors of the material.

Since 1980, Kyriakides and co-workers have conducted experimentally and theoretically investigations into the behavior of pipes subjected to binding with or without external pressure or external pressure only. Kyriakides and Shaw (1982) experimentally tested the response and stability of elastoplastic pipes subjected to both bending and external pressure. In addition, the Ramberg-Osgood relation and the principle of virtual work were used for determining the interaction stability boundaries for moment-pressure or curvature-pressure. Thereafter, Shaw and Kyriakides (1985) experimentally and theoretically extended the analysis of the inelastic tubes to cyclic bending. They demonstrated that reverse bending and subsequent repeated cyclic bending cause a gradual growth of the ovalization of a tube cross-section. Kyriakides and Shaw (1987) performed an experimental investigation on the response and stability of thin-walled tubes subjected to cyclic bending. Their results indicated that under curvature-symmetric loading, the tube progressively ovalizes to a critical value at which it buckles. The critical value of the ovalization was shown to be approximately equal to the value obtained just prior to buckling subjected to monotonic bending. Corona and Kyriakides (1988) investigated the stability of long metal tubes subjected to combined bending and external pressure. The curvature-pressure interaction collapse envelopes were generated for two different loading paths, involving bending followed by pressure and pressure followed by bending. The investigation found that the loading path strongly influences the shape of the envelopes of curvature-pressure interaction. Corona and Kyriakides (1991) experimentally studied the degradation and buckling of circular tubes subjected to cyclic bending and external pressure. They established the effect of the cyclic bending history and of the external pressure on the rate of ovalization and the onset of instability. Kyriakides and Ju (1992a, 1992b) experimentally and theoretically studied the bifurcation and localization instabilities in circular cylindrical shells subjected to pure bending. They discovered that the thinner shells develop short-wavelength periodic ripples on the compressive side of the shell and buckle soon after the ripples appear. However, thickener shells exhibit a limit load instability, as a direct consequence of the ovalization of the shell cross-section caused by bending.

Yeh and Kyriakides investigated the collapse of inelastic thick-walled tubes subjected to external pressure (1986) and studied the collapse of deep water pipes (1988). They found that the major factors that affect the collapse pressure of pipes are the diameter-to-thickness ratio (D/t), Young's modulus and the yield stress of the material in the circumferential direction, initial imperfections in the form of the ovality, and wall thickness variations. Dyau and Kyriakides (1993) investigated the localization of the collapse in cylindrical shells under external pressure. Their research addressed the mechanism of collapse triggered by the limit load instability. It was found that following the limit load the collapse quickly localizes to a section of the shell a few diameters long. The deformations and stresses in the region of localization grow with the decreasing overall pressure, whereas the rest of structure remains intact and retains only a small residual effect from the limit load instability. Dyau and Kyriakides (1993) further investigated the propagation pressure of a long cylindrical shell under external pressure. The propagation pressure is the lowest pressure at which the buckle will propagate. For common structural metal tubes with D/t of less than 100, the propagation pressure is typically half an order of magnitude lower than the collapse pressure of the intact tubes. Dyau and Kyriakides suggested that the design of tubular structures to be subjected to external pressure loading requires the knowledge of the collapse and propagation pressures. Park and Kyriakides (1996) experimentally and theoretically studied the collapse of dented cylinders under external pressure. They found that the collapse of cylinders is relatively sensitive to the geometry of a dent but is critically dependent on the maximum ovalization of its most deformed cross section.

For pipes subjected to combined axial tension and external pressure, some earlier studies were conducted to establish a design criteria for oil well casting (Stuiver and Tomalin 1959, Kyogoku *et al.* 1981, Tamano 1982). However, these earlier studies were limited to examine the path of axial tension followed by external pressure (depicted as the $T \rightarrow P$ path). The collapse strength on initial geometric imperfections and the effect of the stress-strain behavior on the collapse envelope were not dealt with in these studies. Madhavan *et al.* (1993) also investigated the collapse of long, thick-walled tubes for 304 stainless steel subjected to combined axial tension and external pressure. Collapse envelopes for two different loading paths were considered in their study: the $T \rightarrow P$ path and $P \rightarrow T$ path (external pressure followed by axial tension). Collapse tests involving initially ovalized tubes were also carried out. For a theoretical analysis, a two-dimensional elasto-plastic model was used to predict the collapse strength. The experimental results demonstrated that the shape of the stress-strain curve has a significant influence on the tension-pressure collapse envelope and that the collapse strength is strongly influenced by initial ovality.

It has been shown from experimental investigations that engineering alloys such as 304 and 316 stainless steels and high-strength titanium alloys, exhibit viscoplastic behavior (Krempl 1979, Kujawski and Krempl 1981, Ikegami and Ni-Itsu 1983). Therefore, once a pipe is fabricated using the aforementioned metals, it is manipulated under bending with different loading-rates, the response of the metal tube for each loading-rate is expected to generate differently (Pan and Her 1998). Moreover, if the metal tube is loaded under the conditions of external pressure and axial tension, the envelope's shape for pressure-tension interaction will be strongly influenced by a different strain-rate during axial tension. Although no experimental results involving the viscoplastic response for metal tubes under external pressure and axial tension has been accomplished, a theoretical investigation can be carried out by using an available viscoplastic model.

In 1980, Valanis (1980) reformulated the definition of intrinsic time by the plastic strain tensor, the extended endochronic theory has been applied widely and successfully to simulate various material responses subjected to diverse loading histories, elasto-plastic deformation (Watanabe and Atluri 1985, Wu *et al.* 1990, Peng and Ponter 1993, Pan and Chern 1997), creep (Watanabe and Atluri 1986, Wu and Ho 1995, Pan and Chiang 1998, Pan *et al.* 1999), and finite deformation (Im and Atluri 1987, Wu *et al.* 1995, Pan *et al.* 1996, Pan 1997). To investigate circular tubes subjected to bending, Pan and Leu (1997) used the endochronic theory to investigate the collapse of thin-walled tubes. The experimental data on 6061-T6 aluminum and 1018 steel tubes subjected to cyclic bending tested by Kyriakides and Shaw (1987) were compared with the theoretical simulation. Pan and Hsu (1999) and Lee and Pan (2001) also used the endochronic theory to study the viscoplastic behavior of circular tubes subjected to cyclic bending. The experimental data of AISI 304 stainless steel and titanium alloy tubes subjected to cyclic bending with different curvature-rates tested by Pan and Hsu (1999) and Lee and Pan (2001), respectively, were compared with the theoretical simulation. Furthermore, Pan and Lee (2002) investigated the effect of mean curvature on the response of AISI 304 stainless steel tubes subjected to cyclic bending. The endochronic theory was used as the theoretical formulation to simulate their experimental results.

In this study, we employ the first-order ordinary differential constitutive equations of the theory obtained by Murakami and Read (1989) together with the rate-sensitivity function proposed by Pan and Chern (1997) to investigate the viscoplastic collapse of thick-walled tubes subjected to external pressure and axial tension. The principle of virtual work is used to formulate the problem; the relationship among the bending moment, the curvature, and the ovalization is obtained from the necessary equilibrium equations. The collapse envelopes for two different loading paths (the $T \rightarrow P$ path and $P \rightarrow T$ path) were considered, simultaneously. The experimental data of long, thick-walled tubes for 304 stainless steel subjected to combined axial tension and external pressure, which was tested by Madhavan *et al.* (1993), were used in the endochronic simulation. A satisfactory description was achieved by comparing the experimental data of Madhavan *et al.* with the theoretical simulation.

Finally, an investigation based on the endochronic theory was performed to examine the viscoplastic behavior of long, thick-walled tubes of 304 stainless steel subjected to combined axial tension and external pressure. It is demonstrated from the uniaxial stress-strain curve under different strain-rates that the material hardens when the strain-rate increases. Therefore, the magnitude of the limit pressure at collapse increases for the $T \rightarrow P$ loading path and the magnitude of the limit axial tension at collapse increases for the $P \rightarrow T$ loading path. Furthermore, because the metal tube of 304 stainless steel hardens under a faster strain-rate during uniaxial tension, the sizes of the tension-pressure collapse envelope for $T \rightarrow P$ and pressure-tension collapse envelope for $P \rightarrow T$ loading path both increase.

2. Problem formulation

In this section, we formulate the problem of response for a circular tube subjected to external pressure and axial tension. The kinematics of the tube cross section, the constitutive model for elasto-plastic response, and the principle of virtual work are discussed separately as follows.

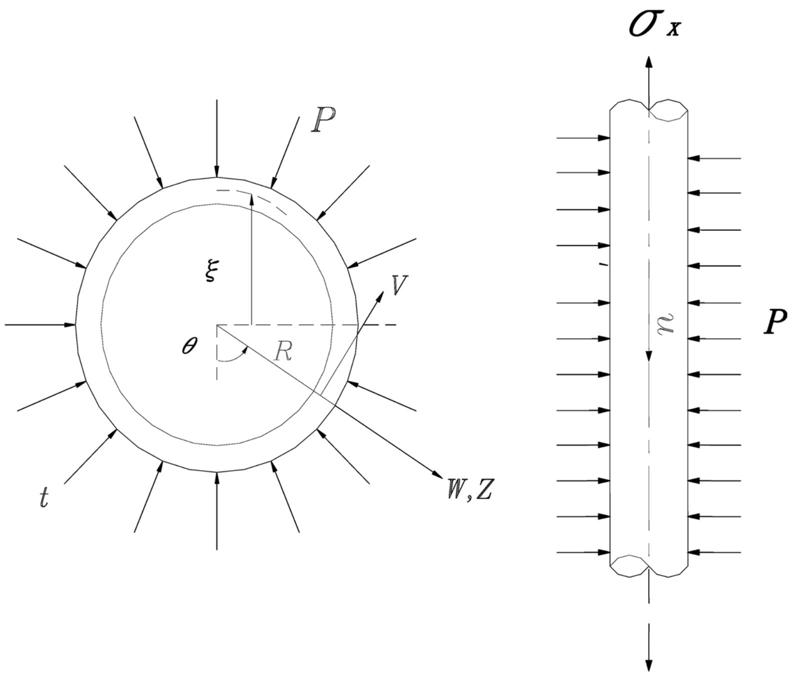

Fig. 1 Problem geometry

2.1 Kinematics

A circular tube subjected to external pressure and axial tension is considered in this study. Fig. 1 shows the problem geometry, in which P is the applied external pressure, R is the mean radius, and t is the wall thickness. Based on the axial, the circumferential, and the radial coordinates x, θ, and r, respectively, the displacement of a point on the tube's mid-surface are denoted as u, v and w, respectively. The plane sections are assumed here to be perpendicular to the tube mid-surface before and during deformation. In addition, the strains are assumed to remain small. The circumferential strain of the deformation is expressed as (Shaw and Kyriakides 1985, Kyriakides and Ju 1992b):

$$\varepsilon_\theta = \varepsilon_\theta^0 + r\kappa_\theta \tag{1}$$

where

$$\varepsilon_\theta^0 = \frac{(v' + w)}{r} + \frac{1}{2}\left(\frac{v' + w}{r}\right)^2 + \frac{1}{2}\left(\frac{v - w'}{r}\right)^2 \tag{2}$$

and

$$k_\theta = \left(\frac{v' - w''}{R^2}\right) \Big/ \sqrt{1 - \left(\frac{v - w'}{R}\right)^2} \tag{3}$$

The axial strain is expressed as

$$\varepsilon_x = \varepsilon_x^0 + \xi \cdot \kappa \tag{4}$$

and

$$\xi = (R + w)\cos\theta - v\sin\theta + z\cos\theta \tag{5}$$

where ε_x^0 is the axial strain of the cylinder's axis. Note that the amount of ε_x^0 is generally not zero, due to the shifting of the neutral axis under external pressure.

2.2 Endochronic constitutive equations

The endochronic theory is adopted for simulating the elasto-plastic response of a long, circular tube subjected to cyclic bending and external pressure. Owing to the highly non-proportional path of the stress history, the incremental form of endochronic theory should be considered to formulate the problem. According to the condition of small deformation for homogeneous and isotropic materials, the increment of the deviatoric stress tensor $d\,\underset{\sim}{s}$ of the endochronic theory is given as (Valanis 1980)

$$d\,\underset{\sim}{s} = 2\rho(0)\,d\,\underset{\sim}{e}^p + 2\underset{\sim}{h}(z)\,dz \tag{6}$$

and

$$\underset{\sim}{h}(z) = \int_0^z \frac{d\rho(z-z')}{dz}\frac{\partial \underset{\sim}{e}^p}{\partial z'} \tag{7}$$

where z is the intrinsic time scale, $\rho(z)$ is termed the kernel function, and $\underset{\sim}{e}^p$ is the deviatoric plastic strain tensor which is defined as

$$d\underset{\sim}{e}^p = d\underset{\sim}{e} - \frac{d\underset{\sim}{s}}{2\mu_0} \tag{8}$$

where $\underset{\sim}{e}$ denotes the deviatoric strain tensor, μ_0 is the elastic shear modulus. The intrinsic time measure ζ is

$$d\zeta = k\left\|d\underset{\sim}{e}^p\right\| \quad \text{or} \quad d\zeta^2 = k^2 d\underset{\sim}{e}^p \cdot d\underset{\sim}{e}^p \tag{9a,b}$$

in which $\|\cdot\|$ represents the Euclidean norm, and k is the rate-sensitivity function. The function k for describing the viscoplastic behavior of material subjected to multiaxial loading is expressed as (Pan and Chern 1997):

$$k = 1 - k_s \quad \log\left(\frac{\dot{e}^p_{eq}}{(\dot{e}^p_{eq})_o}\right) \tag{10}$$

where k_s is a rate-sensitivity parameter, $(\dot{e}^p_{eq})_o$ is the reference equivalent deviatoric plastic strain-rate and $(\dot{e}^p_{eq})$ is the relative equivalent deviatoric plastic strain-rate. The material function (or hardening function) $f(\zeta)$ is

$$f(\zeta) = \frac{d\zeta}{dz} = 1 - Ce^{-\beta\zeta}, \text{ for } C < 1 \tag{11}$$

in which C and β are material parameters. If the plastically incompressible is satisfied, the elastic hydrostatic response can be written as

$$d\sigma_{kk} = 3Kd\varepsilon_{kk} \tag{12}$$

where σ_{kk} and ε_{kk} are the traces of stress and strain tensors, respectively, and K is the elastic bulk modulus. According to the mathematical characteristic of the kernel function $\rho(z)$, Eq. (6) is expressed as (Murakami and Read 1989, Pan *et al.* 1996, Pan and Chern 1997)

$$d\underset{\sim}{s} = \sum_{i=1}^{n} d\underset{\sim}{s}_i = 2\sum_{i=1}^{n} C_i d\underset{\sim}{e}^p - \sum_{i=1}^{n} \alpha_i \underset{\sim}{s}_i dz \tag{13}$$

where C_i and α_i are material constants. Substituting Eq. (8) into Eq. (13) leads to

$$d\underset{\sim}{s} = \frac{\mu_0}{\mu_0 + \sum_{i=1}^{n} C_i}\left[2\sum_{i=1}^{n} C_i d\underset{\sim}{e} - \sum_{i=1}^{n} \alpha_i \underset{\sim}{s}_i dz\right] \tag{14}$$

By using Eq. (12), Eq. (14) can be expressed in terms of the stress and strain tensors as

$$d\underset{\sim}{\sigma} = p_1 d\underset{\sim}{\varepsilon} + p_2 d\varepsilon_{kk}\underset{\sim}{I} + p_3 \sum_{i=1}^{n} \alpha_i \left(\underset{\sim}{\sigma} - \frac{\sigma_{kk}}{3}\underset{\sim}{I}\right)_i dz \tag{15}$$

where

$$p_1 = \frac{2\rho(0)}{1 + \dfrac{\rho(0)}{\mu_0}}, \quad p_2 = K - \frac{2\rho(0)}{3\left(1 + \dfrac{\rho(0)}{\mu_0}\right)}, \quad p_2 = \frac{1}{1 + \dfrac{\rho(0)}{\mu_0}} \tag{16}$$

2.3 Thick-walled tube under uniaxial tension

The stress and strain tensors are

$$\underset{\sim}{\sigma} = \begin{bmatrix} \sigma_x & 0 & 0 \\ 0 & 0 & 0 \\ 0 & 0 & 0 \end{bmatrix}, \quad \underset{\sim}{\varepsilon} = \begin{bmatrix} \varepsilon_x & 0 & 0 \\ 0 & \varepsilon_\theta & 0 \\ 0 & 0 & \varepsilon_r \end{bmatrix} \tag{17a,b}$$

in which x-direction, r-direction and θ-direction indicate the axial, circumferential and radial directions, respectively. For the isotropic and homogeneous material, the magnitude of ε_r is equal to the magnitude of ε_θ for uniaxial tension. From Eq. (8), the deviatoric plastic strain tensor is determined to be

$$d\underset{\sim}{e}^p = \begin{bmatrix} \frac{2}{3}\left(d\varepsilon_x - d\varepsilon_r - \frac{d\sigma_x}{2\mu_0}\right) & 0 & 0 \\ 0 & \frac{-1}{3}\left(d\varepsilon_x - d\varepsilon_r - \frac{d\sigma_x}{2\mu_0}\right) & 0 \\ 0 & 0 & \frac{-1}{3}\left(d\varepsilon_x - d\varepsilon_r - \frac{d\sigma_x}{2\mu_0}\right) \end{bmatrix} \tag{18}$$

Eq. (15) can be extended to:

$$d\sigma_x = p_1 d\varepsilon_x + p_2(d\varepsilon_x + 2d\varepsilon_r) + \frac{2}{3}p_3 \sum_{i=1}^{n} \alpha_i (\sigma_x)_i dz \tag{19}$$

$$0 = p_1 d\varepsilon_x + p_2(d\varepsilon_x + 2d\varepsilon_r) - \frac{1}{3}p_3 \sum_{i=1}^{n} \alpha_i (\sigma_x)_i dz \tag{20}$$

where p_1, p_2 and p_3 are defined in Eq. (16). From Eq. (20), we obtain

$$d\varepsilon_r = p_a d\varepsilon_x + p_b dz \tag{21}$$

in which

$$p_a = \frac{-p_2}{p_1 + 2p_2}, \quad p_b = \frac{p_3}{3(p_1 + 2p_2)} \sum_{i=1}^{n} \alpha_i (\sigma_x)_i \tag{22}$$

Using Eq. (21) in (19), we obtain

$$d\varepsilon_x = p_c d\sigma_x + p_d dz \tag{23}$$

where

$$p_c = \frac{1}{p_1 + p_2 + 2p_2 p_a}, \quad p_d = \frac{-2p_2 p_b - \frac{2}{3} p_3 \sum_{i=1}^{n} \alpha_i (\sigma_x)_i}{p_1 + p_2 + 2p_2 p_a} \tag{24}$$

Substituting Eq. (23) into (21), we have

$$d\varepsilon_r = p_a p_c d\sigma_x + (p_b + p_d) dz \tag{25}$$

Based on the definition of intrinsic time measure ζ in Eq. (9b), we write

$$d\zeta^2 = \frac{4}{9} k^2 \left(d\varepsilon_x - d\varepsilon_r - \frac{d\sigma_x}{2\mu_0} \right)^2 \tag{26}$$

The quantities of $d\varepsilon_x$ and $d\varepsilon_r$ are expressed by input known value of $d\sigma$ and output calculated value of dz in Eqs. (23) and (25), respectively. In addition, the intrinsic time measure ζ is expressed by known value of $f(\zeta)$ and output calculated value of dz in Eq. (11). By rearranging Eq. (26), a quadratic form with the variable dz can be obtained. By definition, the intrinsic time measure ζ in Eq. (9a) is invariably greater than or equal to zero. The expression of $d\zeta$ in Eq. (9b) is expected to generate two roots with opposite signs or a zero value. The material function $f(\zeta)$, as shown in Eq. (11), invariably exceeds zero. Therefore, two roots with opposite sign or a zero value are found in Eq. (26). The positive root of dz is the desired one.

Once the value of dz is determined, the magnitudes of $d\varepsilon_x$ and $d\varepsilon_r$ are calculated from Eqs. (23) and (25), respectively, and the magnitude of $d\zeta$ is calculated from Eq. (11). By updating the values of σ, ε_x, ε_r, ζ, and z, the calculation process is repeated again. Thus, the entire deformation can be determined systematically.

2.4 Thick-walled tube under external pressure

The stress and strain tensors are

$$\underset{\sim}{\sigma} = \begin{bmatrix} 0 & 0 & 0 \\ 0 & \sigma_\theta & 0 \\ 0 & 0 & \sigma_r \end{bmatrix}, \quad \underset{\sim}{\varepsilon} = \begin{bmatrix} \varepsilon_x & 0 & 0 \\ 0 & \varepsilon_\theta & 0 \\ 0 & 0 & \varepsilon_r \end{bmatrix} \tag{27a,b}$$

From Eq. (8), the deviatoric plastic strain tensor is determined to be

$$\underset{\sim}{e}^{p} = \begin{bmatrix} \frac{2\varepsilon_x - \varepsilon_\theta - \varepsilon_r}{3} + \frac{\sigma_\theta + \sigma_r}{6\mu_0} & 0 & 0 \\ 0 & \frac{2\varepsilon_\theta - \varepsilon_x - \varepsilon_r}{3} - \frac{2\sigma_\theta - \sigma_r}{6\mu_0} & 0 \\ 0 & 0 & \frac{2\varepsilon_r - \varepsilon_x - \varepsilon_\theta}{3} - \frac{2\sigma_r - \sigma_\theta}{6\mu_0} \end{bmatrix} \tag{28}$$

Substitution of Eqs. (27a) and 27(b) into Eq. (15) yields

$$0 = p_1 d\varepsilon_x + p_2(d\varepsilon_x + d\varepsilon_\theta + d\varepsilon_r) - p_3 \sum_{i=1}^{n} \alpha_i \left(\frac{\sigma_\theta + \sigma_r}{3}\right)_i dz \tag{29}$$

$$d\sigma_\theta = p_1 d\varepsilon_\theta + p_2(d\varepsilon_x + d\varepsilon_\theta + d\varepsilon_r) + p_3 \sum_{i=1}^{n} \alpha_i \left(\frac{2\sigma_\theta - \sigma_r}{3}\right)_i dz \tag{30}$$

$$d\sigma_r = p_1 d\varepsilon_r + p_2(d\varepsilon_x + d\varepsilon_\theta + d\varepsilon_r) + p_3 \sum_{i=1}^{n} \alpha_i \left(\frac{2\sigma_r - \sigma_\theta}{3}\right)_i dz \tag{31}$$

Eqs. (29)-(31) are expressed as

$$(p_1 + p_2) d\varepsilon_x + p_2 d\varepsilon_r + p_2 d\varepsilon_\theta = A_1 dz \tag{32}$$

$$p_2 d\varepsilon_x + (p_1 + p_2) d\varepsilon_\theta + p_2 d\varepsilon_r = d\sigma_\theta + A_2 dz \tag{33}$$

$$p_2 d\varepsilon_x + p_2 d\varepsilon_\theta + (p_1 + p_2) d\varepsilon_r = d\sigma_r + A_3 dz \tag{34}$$

where

$$A_1 = p_3 \sum_{i=1}^{n} \alpha_i \left(\frac{\sigma_\theta + \sigma_r}{3}\right)_i, \quad A_2 = -p_3 \sum_{i=1}^{n} \alpha_i \left(\frac{2\sigma_\theta - \sigma_r}{3}\right)_i, \quad A_3 = -p_3 \sum_{i=1}^{n} \alpha_i \left(\frac{2\sigma_r - \sigma_\theta}{3}\right)_i \tag{35a,b,c}$$

When a increment of the external pressure dP is added (input quantity), the magnitudes of $d\sigma_\theta$ and $d\sigma_r$ are determined to be (Timoshenko and Goodier 1970)

$$d\sigma_\theta = \frac{-b^2}{b^2 - a^2}\left[\frac{a^2}{r^2} + 1\right] dP \tag{36}$$

and

$$d\sigma_r = \frac{b^2}{b^2 - a^2}\left[\frac{a^2}{r^2} - 1\right] dP \tag{37}$$

in which a is the inside radius and b is the outside radius. Based on the definition of the intrinsic time measure ζ in Eq. (9b), we have

$$d\zeta^2 = k^2\left[\left(\frac{2\varepsilon_x-\varepsilon_\theta-\varepsilon_r}{3}+\frac{\sigma_\theta+\sigma_r}{6\mu_0}\right)^2+\left(\frac{2\varepsilon_\theta-\varepsilon_x-\varepsilon_r}{3}-\frac{2\sigma_\theta-\sigma_r}{6\mu_0}\right)^2+\left(\frac{2\varepsilon_r-\varepsilon_x-\varepsilon_\theta}{3}-\frac{2\sigma_r-\sigma_\theta}{6\mu_0}\right)^2\right] \quad (38)$$

The quantities of $d\varepsilon_x$, $d\varepsilon_\theta$ and $d\varepsilon_r$ can be expressed by input known values of $d\sigma_\theta$ and $d\sigma_r$ (calculated by Eqs. (36) and (37)) and output calculated value of dz from Eqs. (32), (33) and (34). The intrinsic time measure ζ is expressed by known value of $f(\zeta)$ and output calculated value of dz in Eq. (11). By rearranging Eq. (38), a quadratic form with only one variable dz can be obtained. Similarly, the positive root of dz is the desired one.

Once the value of dz is determined, the magnitudes of $d\varepsilon_x$, $d\varepsilon_\theta$ and $d\varepsilon_r$ are calculated from Eqs. (32), (33) and (34), and the magnitude of $d\zeta$ is calculated from Eq. (11). By updating the values of σ_θ, σ_r, ε_x, ε_θ, ε_r, ζ and z, the calculation process is repeated. Thus, the entire deformation can be determined systematically.

2.5 Principle of virtual work

The principle of virtual work, which satisfies the equilibrium requirement, is given by

$$\int_V \sigma_{ij}\delta\varepsilon_{ij}dV = \delta W \quad (39)$$

where V is the volume of the material of the tube section considered, and δW is the virtual work of the external loads. For the case of thick-walled tube subjected to axial tension, the quantity of δW is expressed for the incremental loading to be

$$\int_V (\sigma_{ij}+\dot{\sigma}_{ij})\delta\dot{\varepsilon}_{ij}dV$$

$$= 2R\int_0^{\pi}\int_{-t/2}^{t/2}[\hat{\sigma}_x\delta\dot{\varepsilon}_x]dTd\theta = 0 \quad (40)$$

where $\hat{\sigma}_x = \sigma + \sigma_x$ and $(\dot{\ })$ denotes the increment of $(\ )$. For the case involving a circular tube subjected to external pressure, Eq. (39) is written as (Kyriadies and Shaw 1987)

$$\int_V (\sigma_{ij}+\dot{\sigma}_{ij})\delta\dot{\varepsilon}_{ij}dV = 2R\int_0^{\pi}\int_{-t/2}^{t/2}[\hat{\sigma}_\theta\delta\dot{\varepsilon}_\theta+\hat{\sigma}_r\delta\dot{\varepsilon}_r]dTd\theta$$

$$= \hat{P}R\int_0^{2\pi}\left[\delta\dot{w}+\frac{1}{2R}(2\hat{w}\delta\dot{w}+2\hat{v}\delta\dot{v}+\hat{w}\delta\dot{v}'+\hat{v}'\delta\dot{w}-\hat{v}\delta\dot{w}'-\hat{w}'\delta\dot{v})\right]d\theta \quad (41)$$

where $\hat{P}_x = P+\dot{P}$, $\hat{v} = v+\dot{v}$, etc. The in-plane displacement v and w are assumed to be symmetrical and are approximated by the following expression (Shaw and Kyriakides 1985, Kyriakides and Shaw 1987):

$$v \cong R \sum_{n=2}^{N} a_n \sin n\theta, \quad w \cong R \sum_{n=0}^{N} b_n \cos n\theta \tag{42a, b}$$

where the number of terms N is chosen to ensure satisfactory convergence. Kyriakides and Shaw (1987) investigated the sensitivity of the moment-curvature and ovalization-curvature response for monotonic pure bending to the number of expansion terms used in Eqs. (42a) and (42b). Those equations clearly indicate that N = 4 or 6 is sufficient. By substituting Eqs. (1)-(5), (42a) and (42b) into Eq. (40) or (41), a system of $2N$ + 1 nonlinear algebraic equations in terms of $\dot{a}_2, \dot{a}_3, \ldots, \dot{b}_0, \dot{b}_1, \dot{b}_2, \ldots, \varepsilon_x^0$ are determined. This system of equations is solved using the Newton-Raphson method. The iterative scheme contains nested iterations for the constitutive relations. Kyriakides and Shaw (1987) provide a more detailed derivation of the system of equations.

3. Comparisons and discussions

In this section, the collapse of thick-walled tubes subjected to external pressure and axial tension is investigated theoretically. Experimental data of thick-walled tubes for 304 stainless steel tested by Madhavan *et al.* (1993) were compared with the theoretical simulation. Finally, by using the rate-sensitivity function in the theory, the analysis was theoretically extended to investigate the viscoplastic collapse. In the theoretical study, the kernel function of the endochronic theory was considered to compose by three terms of exponentially decaying function, therefore, the material parameters of the theory can be determined according to the method proposed by Fan (1983). The material parameters were determined to be: μ_0 = 7.63 × 10^4 MPa, K = 1.75 × 10^5 MPa, C_1 = 1.7 × 10^6 MPa, α_1 = 9000, C_2 = 1.5 × 10^5 MPa, α_2 = 730, C_3 = 2.4 × 10^3 MPa, α_3 = 135, C = 0.15, β = 20 and k_s = 0.045. Fig. 2 shows schematically the two different loading paths adopted in their experiment (Madhavan *et al.* 1993). For the first loading path, the axial tension is applied to a certain level; then, with the tension held constant, the tube is pressured until it collapses (denoted as the $T \rightarrow P$ path). For the second loading path, the pressure is applied to a certain level; then, with the pressure held constant, the tube is tensioned until it collapses (denoted as the $P \rightarrow T$ path).

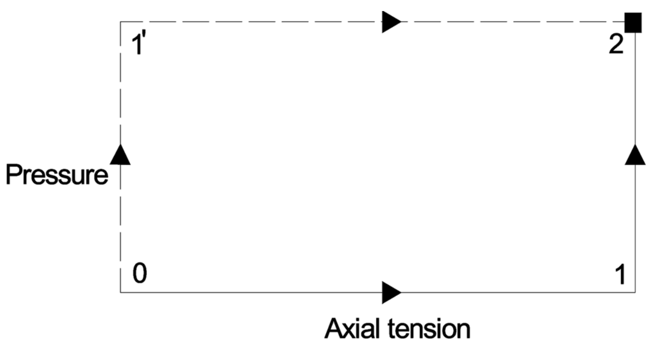

Fig. 2 $T \rightarrow P$ loading path (0→1→2) and $P \rightarrow T$ loading path (0→1'→2)

3.1 Elastoplastic collapse

Fig. 3 depicts the experimental and theoretical results of the axial stress-strain curve. The theoretical curve in the dotted line was determined by Madhavan *et al.* (1993). It was fitted by a Ramberg-Osgood method. The theoretical curve in the solid line was obtained by using the endochonic theory. Figs. 4-7 give the experimental and theoretical tension-pressure collapse envelopes for specimens with a D_m/t of 38.3, 24.5, 18.2, and 12.2, respectively. The quantity of D_m is the outside diameter and the quantity of t is the wall-thickness. The loading paths are the $T \rightarrow P$ paths. The experimental data of pressure at collapse P_{co} and tension at collapse T_c are normalized by $P_o = 2\sigma_o t/D_m$ and $T_o = \pi\sigma_o D_m t$, where σ_o is the yield stress at 0.5% strain (Madhavan *et al.* 1993). The trend shows by the experimental results that the collapse pressure decreases with axial tension. It is also shown that when the magnitude of D_m/t ratio is small, the tension-pressure becomes flat. The dotted curves indicate the theoretical calculation by Madhavan *et al.* (1993). The parameter S is the measured anisotropy. The solid curves were determined using the endochronic theory described in previous section. In Fig. 8, the predicted axial strain with tension at collapse is compared with the experiments. These results are for a D_m/t of 24.5 and the loading path of $T \rightarrow P$ path. It can be seen that the axial strain with tension at collapse increases rapidly for higher tension at collapse. Fig. 9 depicts the experimental and theoretical results of the collapse pressure as a function the initial ovality. These results are for a D_m/t of 26.7 and the loading path of $T \rightarrow P$ path, and at a relatively low prescribed tension of T_c/T_o = 0.16. It can be observed that the collapse pressure drops by as much as 40% at 1% of initial ovality. It can be observed that the endochronic approach correlates better with the experimental results than the simulation reported by Madhavan *et al.* (1993).

Since the interaction between collapse pressure and tension depends on the nonlinear material behavior, the collapse envelope is likely to be affected by the tension-pressure loading sequence. Madhavan *et al.* (1993) experimentally investigated tension-pressure collapse envelopes for tubes

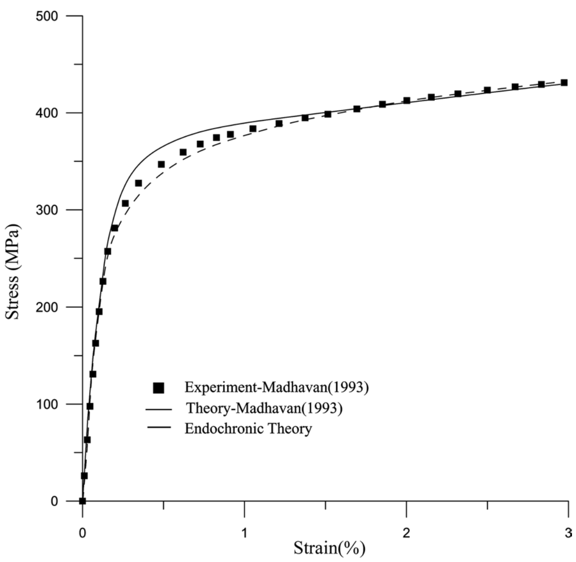

Fig. 3 Experimental and theoretical uniaxial stress-strain curves for 304 stainless steel

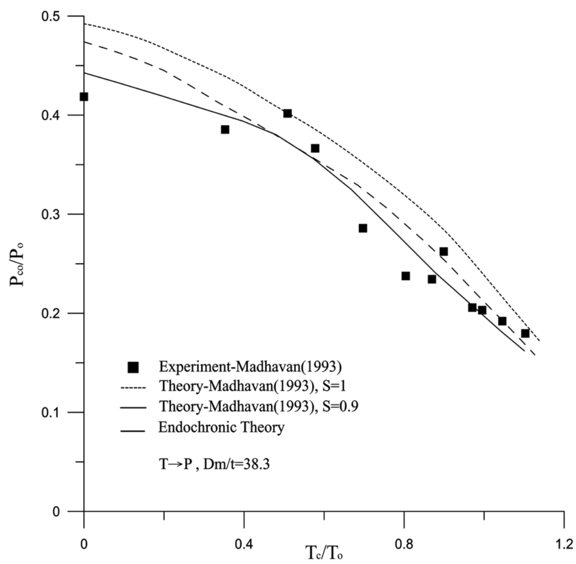

Fig. 4 Experimental and theoretical tension-pressure envelopes ($T \rightarrow P$), for D_m/t = 38.3

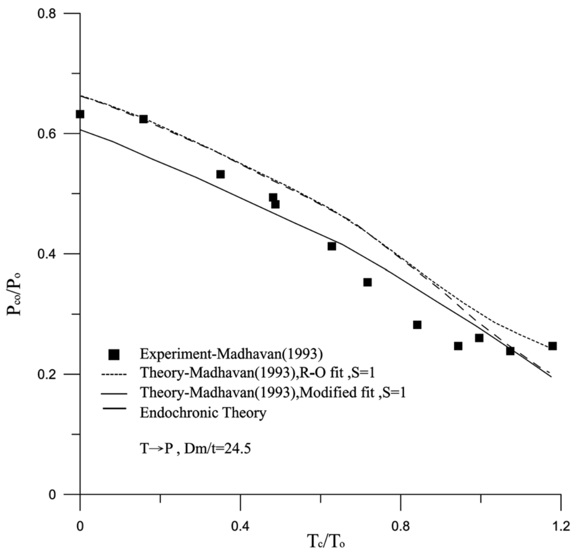

Fig. 5 Experimental and theoretical tension-pressure collapse envelopes ($T \rightarrow P$), for D_m/t = 24.5

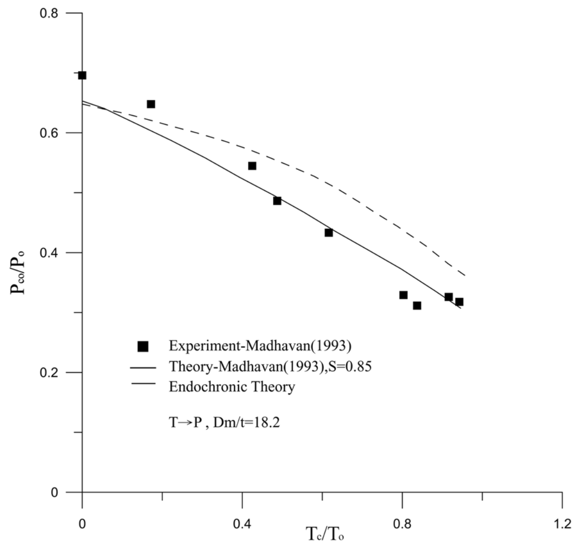

Fig. 6 Experimental and theoretical tension-pressure collapse envelopes ($T \rightarrow P$), for D_m/t = 18.2

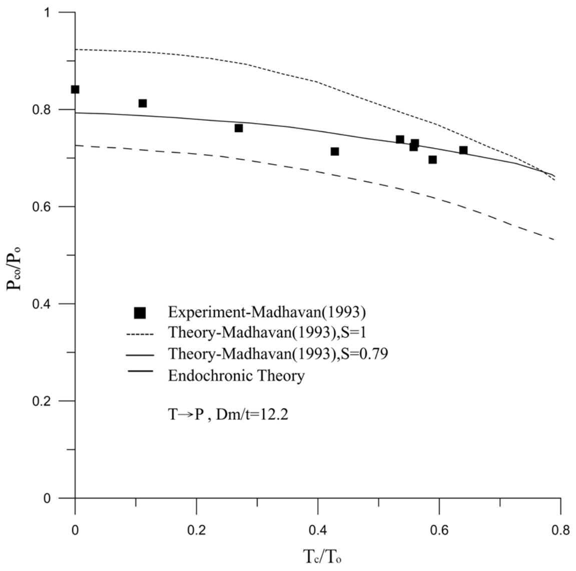

Fig. 7 Experimental and theoretical tension-pressure collapse envelopes ($T \rightarrow P$), for D_m/t = 12.2

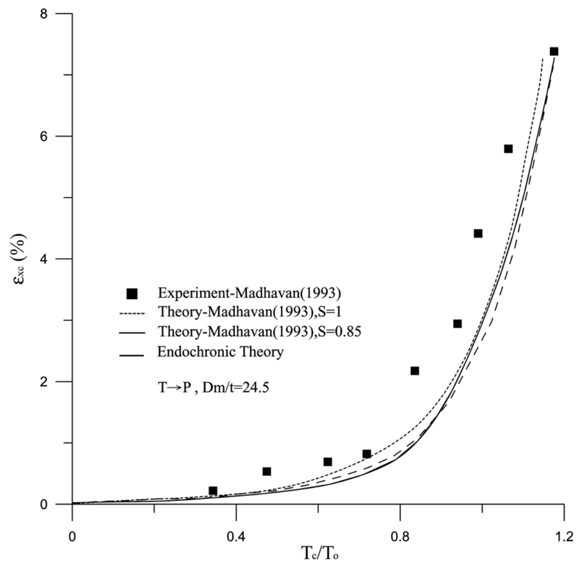

Fig. 8 Experimental and theoretical axial strain at collapse-tension at collapse envelopes ($T \rightarrow P$), for D_m/t = 12.2

with a D_m/t of 27.2 under the $P \rightarrow T$ loading path shown in Fig. 10 (This is the only experimental case of the $P \rightarrow T$ loading path in their paper). The dotted curves indicate the theoretical calculation by Madhavan *et al.* (1993) with S = 0.77. The solid curves were determined using the endochronic theory described in previous section. Due to none of the experimental data for same D_m/t ratio subjected to two loading paths, endochronic simulations were used to determine the tension-pressure

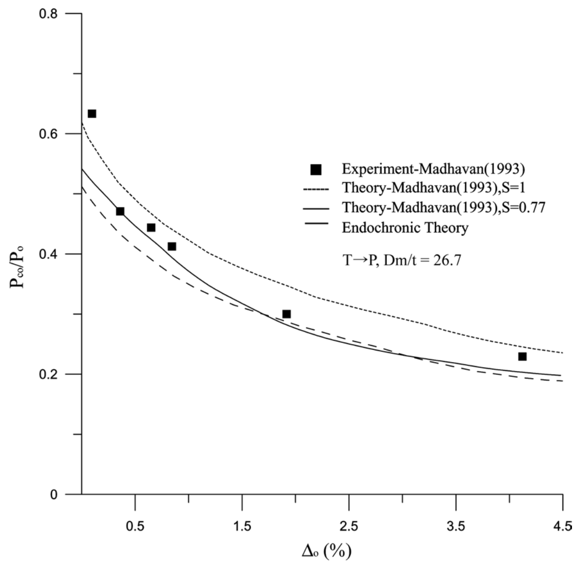

Fig. 9 Experimental and theoretical collapse strength of initially ovalized tubes ($T \rightarrow P$, D_m/t = 26.7, T_c/T_o = 0.16)

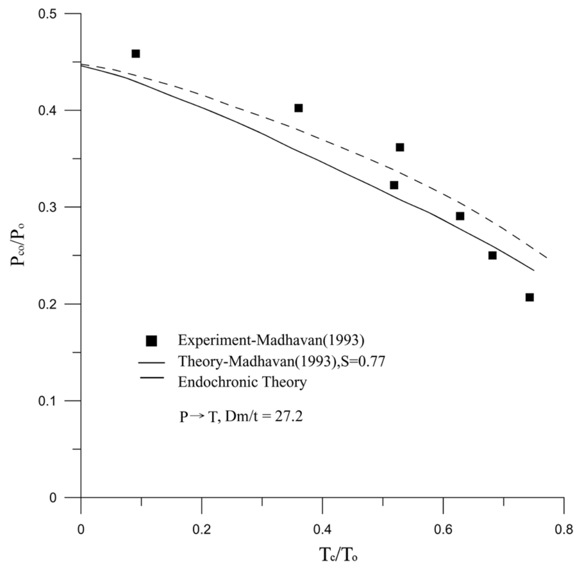

Fig. 10 Experimental and theoretical pressure-tension collapse envelopes ($P \rightarrow T$), for D_m/t = 27.2

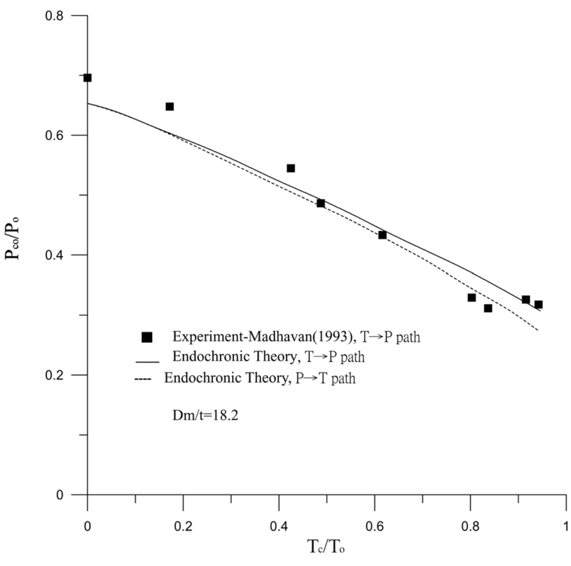

Fig. 11 Effect of loading path on tension-pressure collapse envelope (D_m/t = 18.2)

collapse envelopes of both loading paths for comparison. Fig. 11 shows experimental and theoretical tension-pressure collapse envelopes for specimens with a D_m/t of 18.2 under the experimental $T \rightarrow P$ loading path, the endochronic theoretical $T \rightarrow P$ loading path and the endochronic theoretical $P \rightarrow T$ loading path. The theoretical predictions are included $P \rightarrow T$, and $T \rightarrow P$ loading paths. These results illustrate that the effect of the loading path on the tension-pressure collapse envelope is not significant for the D_m/t range of interest.

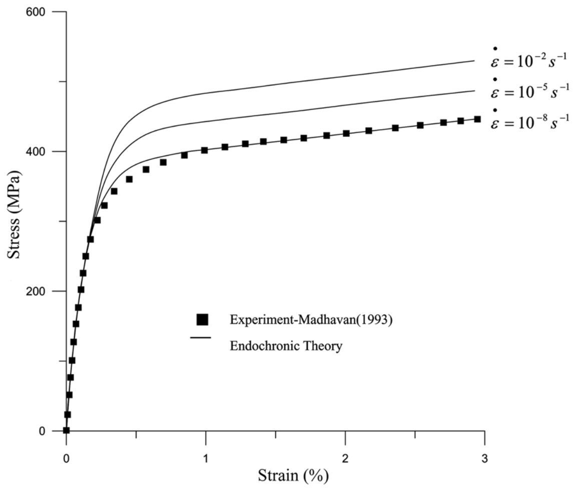

Fig. 12 Predicted uniaxial stress-strain curves under three different strain-rates

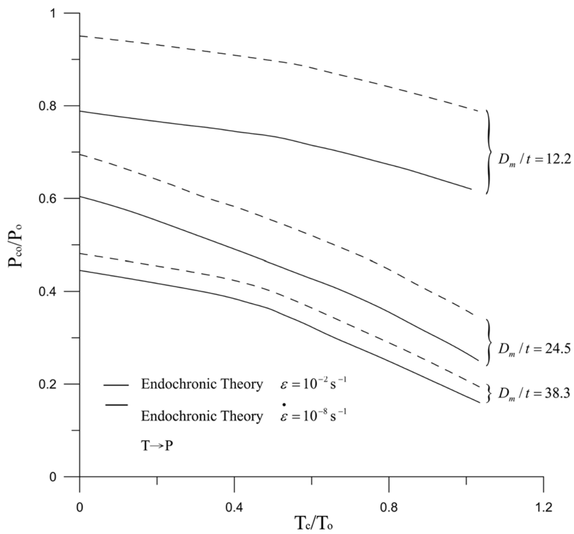

Fig. 13 Predicted tension-pressure collapse envelopes ($T \to P$) under two different strain-rates, for D_m/t = 38.3, 24.5 and 12.2

3.2 Viscoplastic collapse

Based on the endochronic constitutive equations with rate-sensitivity function in section 2, our investigation was extended to consider the viscoplastic collapse of thick-walled tubes subjected to external pressure and axial tension. Because the same material (304 stainless steel) was used in the endochronic viscoplastic simulation by Pan and Chern (1997), the parameter k_a of the rate-sensitivity function is taken as 0.045. If we assume that the experimental data during the axial tension were conducted by a slow strain-rate of 10^{-8} s^{-1}. Based on the endochronic theory with the rate-sensitivity function, the theoretical simulations are considered for an axial tension with a fast strain-rate of 10^{-2} s^{-1}. Fig. 12 depicts the predicted results of the axial stress-strain curves for three different strain-rates of 10^{-8}, 10^{-5}, and 10^{-2} s^{-1}. This figure shows that the stress-strain curves are sensitive to the value of the strain-rate: the faster the strain-rate is, the faster the degree of hardening. Due to the hardening of the tube at higher strain-rate, the magnitudes of the pressure and axial tension at collapse increase. Fig. 13 demonstrates the predicted results of tension-pressure collapse envelopes for tubes with different D_m/t of 38.3, 24.5, and 12.2 for two different strain-rates of 10^{-8} s^{-1} and 10^{-2} s^{-1}. The loading path is the $T \to P$ path. It can be seen that the collapse envelopes move upward when a higher strain-rate is applied. Furthermore, the lower the magnitude of D_m/t is, the wider the distance between the two collapse envelopes for the two different strain-rates. A similar phenomenon is observed from the predicted collapse envelope for tubes with a D_m/t of 27.2 under the $P \to T$ loading path at two different strain-rates, as shown in Fig. 14.

3.3 Discussion

It can be seen from Figs. 3-9 that the theory used by Madhavan *et al.* (1993) also predicted the collapse envelopes for two loading paths. However, six groups of material parameters were

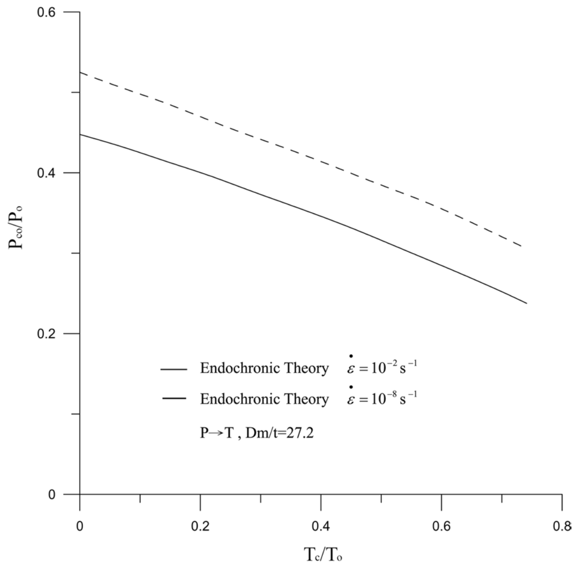

Fig. 14 Predicted pressure-tension collapse envelopes ($P \rightarrow T$) under two different strain-rates, for D_m/t = 27.2

determined to simulate six groups of tubes with different D_m/t ratios. Furthermore, the anisotropic parameter S was used to indicate the yield anisotropies of tubes due to the manufacturing process. A method (Kyriakides and Yeh 1988) was used by them to characterize and model such yield anisotropies. The consideration of so many groups of material parameters for a single metal tube and the process of determining the anisotropic parameter, S, makes the model used by Madhavan *et al.* (1993) complicated and inconvenience. In addition, 304 stainless steel has been shown to have viscoplastic behavior. Therefore, a theoretical prediction should be capable of simulating the viscoplastic effect. However, the model used by Madhavan *et al.* (1993) does not include this function. On the other hand, the endochronic theory uses only one group of material parameters, and it can be extended to describe the viscoplastic collapse (Figs. 13 and 14). Moreover, our simulations based on the endochronic theory correlate better with the experimental data than the theoretical simulations conducted by Madhavan *et al.* (1993).

4. Conclusions

The first-order differential constitutive equations of the endochronic theory with the rate-sensitivity function of the intrinsic time measure were used to investigate the collapse of thick-walled tubes subjected to external pressure and axial tension. The prediction was compared with the experimental and theoretical data reported in Madhavan *et al.* (1993). Several important conclusions can be drawn from our work.

(1) The endochronic theory can be extended to describe the collapse of thick-walled tubes subjected to external pressure and axial tension. In this study, the prediction by the theory for two loading paths ($T \rightarrow P$ and $P \rightarrow T$ paths) correlates well with the experimental data shown in Figs. 3-10.

(2) Although the model used by Madhavan *et al.* (1993) can also predict the collapse of thick-walled tubes subjected to external pressure and axial tension, the necessity of six different groups of material parameters for six different groups of D_m/t ratios, as well as an extra anisotropic parameter, makes their model complicated and inconvenient. However, the endochronic model requires only one group of material parameters to simulate the collapse of thick-walled tubes with different D_m/t ratios subjected to external pressure and axial tension.

(3) By using the rate-sensitivity function, the endochronic theory can be used to simulate the viscoplastic behavior. In this paper, this approach was used to describe the viscoplastic collapse of thick-walled tubes subjected to external pressure and axial tension. It can be seen from Fig. 13 that the collapse envelopes move upward when a higher strain-rate is applied for the $T \rightarrow P$ loading path. Furthermore, the lower the magnitude of a D_m/t, the wider the distance between the two collapse envelopes for the two different strain-rates is. In addition, for the $P \rightarrow T$ loading path, a similar phenomenon can also be found (Fig. 14).

Acknowledgements

The work presented was carried out with the support of National Science Council under grant NSC 90-2212-E-269-001. Its support is gratefully acknowledged.

References

Corona, E. and Kyriakides, S. (1988), "On the collapse of inelastic tubes under combined bending and pressure", *Int. J. Solids Struct.*, **24**(5), 505-535.

Corona, E. and Kyriakides, S. (1991), "An experimental investigation of the degradation and buckling of circular tubes under cyclic bending and external pressure", *Thin-Walled Struct.*, **12**, 229-263.

Dyau, J.Y. and Kyriakides, S. (1993), "On the propagation pressure of long cylindrical shells under external pressure", *Int. J. Mech. Sci.*, **35**, 675-713.

Fan, J. (1983), "A comprehensive numerical study and experimental verification of endochronic plasticity", Ph.D. Dissertation, Department of Aerospace Engineering and Applied Mechanics, University of Cincinnati.

Ikegami, K. and Ni-Itsu, Y. (1983), "Experimental evaluation of the interaction effect between plastic and creep deformation", *Proc. of Plasticity Today Symposium*, Udine, Italy, 27-30.

Im, S. and Atluri, S.N. (1987), "A study of two finite strain plasticity models: An internal time theory using Mandel's director concept and a general isotropic/kinematic-hardening theory", *Int. J. Plasticity*, **3**, 163-191.

Krempl, E. (1979), "An experimental study of room-temperature sensitivity, creep and relaxation of AISI 304 stainless steel", *J. Mech. Phys. Solids*, **27**, 363-375.

Kujawski, D. and Krempl, E. (1981), "The rate(time)-dependent behavior of $Ti_7Al_2Cb_1Ta$ titanium alloy at room temperature under quasi-static monotonic and cyclic loading", *J. Appl. Mech.*, ASME, **48**, 55-63.

Kyogoku, T., Tokimasa, K., Nakanishi, H. and Okazawa, T. (1981), "Experimental study on the effect of axial tension load on the collapse strength of oil well casing", *OTC 4108*, 387-395.

Kyriakides, S. and Ju, G.T. (1992a), "Bifurcation and localization instabilities in cylindrical shells under bending, - I. Experiments", *Int. J. Solids Struct.*, **29**(9), 1117-1142.

Kyriakides, S. and Ju, G.T. (1992b), "Bifurcation and localization instabilities in cylindrical shells under bending, - II. Predictions", *Int. J. Solids Struct.*, **29**(9), 1143-1171.

Kyriakides, S. and Shaw, P.K. (1982), "Response and stability of elastoplastic circular pipes under combined bending and external pressure", *Int. J. Solids Struct.*, **18**(11), 957-973.

Kyriakides, S. and Shaw, P.K. (1987), "Inelastic buckling of tubes under cyclic loads", *J. Press. Vessel Tech.*, ASME, **109**, 169-178.

Kyriakides, S. and Yeh, M.K. (1988), "Plastic anisotropy in drawn metal tubes", *J. Engng. Ind.*, ASME, **110**,

303-307.
Lee, K.L. and Pan, W.F. (2001), "Viscoplastic collapse of titanium alloy tubes under cyclic bending", *Int. J. Struct. Engng. Mech.*, **11**(3), 315-324.
Madhavan, R., Babcock, C.D. and Singer, J. (1993), "On the collapse of long, thick-walled tubes under external pressure and axial tension", *J. Press. Vessel Tech.*, **115**, 15-26.
Murakami, J. and Read, H.E. (1989), "A second-order numerical scheme for integrating the endochronic plasticity equations", *Comp. Struct.*, **31**, 663-672.
Pan, W.F. (1997), "Endochronic simulation for finite viscoplastic deformation", *Int. J. Plasticity*, **13**(6/7), 571-586.
Pan, W.F. and Chern, C.H. (1997), "Endochronic description for viscoplastic behavior of materials under multiaxial loading", *Int. J. Solids Struct.*, **34**(17), 2131-2159.
Pan, W.F. and Chiang, W.J. (1998), "Endochronic simulation for muitiaxial creep", *Int. Journal*, *Series A*, JSME, **41**(2), 204-210.
Pan, W.F., Chiang, W.J. and Wang, C.K. (1999), "Endochronic analysis for rate-dependent elasto-plastic deformation", *Int. J. Solids Struct.*, **36**, 3215-3237.
Pan, W.F. and Her, Y.S. (1998), "Viscoplastic collapse of thin-walled tubes under cyclic bending", *J. Engng. Mat. Tech.*, ASME, **120**, 287-290.
Pan, W.F. and Hsu, C.M. (1999), "Viscoplastic analysis of thin-walled tubes under cyclic bending", *Int. J. Struct. Engng. Mech.*, **7**(5), 457-471.
Pan, W.F. and Lee K.L. (2002), "The effect of mean curvature on the response and collapse of thin-walled tubes under cyclic bending", *Int. J., Series A*, JSME, **45**(2), 309-318.
Pan, W.F., Lee, T.H. and Yeh. W.C. (1996), "Endochronic analysis for finite elasto-plastic deformation and application to metal tube under torsion and metal rectangular block under biaxial compression", *Int. J. Plasticity*, **12**(10), 1287-1316.
Pan, W.F. and Leu, K.T. (1997), "Endochronic analysis for viscoplastic collapse of thin-walled tube under combined bending and external pressure", *Int. J., Series A*, JSME, **40**(2), 189-199.
Park, T.D. and Kyriakides, S. (1996), "On the collapse of dented cylinders under external pressure", *Int. J. Mech. Sci.*, **38**(5), 557-578.
Peng, X. and Ponter, A.R.S. (1993), "Extremal properties of endochronic plasticity, Part I: Extremal path of the constitutive equation without a yield surface, Part II: Extremal path of the constitutive equation with a yield surface and application", *Int. J. Plasticity*, **9**, 551-581.
Shaw, P.K. and Kyriakides, S. (1985), "Inelastic analysis of thin-walled tubes under cyclic bending", *Int. J. Solids Struct.*, **21**(11), 1073-1110.
Stuiver, W. and Tomalin, P.F. (1959), "The failure of tube under combined external pressure and axial load", *SESA Proc.*, **16**(2), 39-48.
Tamano, T., Mimura, H. and Yanagimoto, S. (1982), "Examination of commercial casing collapse strength under axial loading", *Proc. of the 1st Offshore Mechanics/Artic Engineering/Deep Sea Systems Symposium*, ASME 1, 113-118.
Valanis, K.C. (1980), "Fundamental consequence of a new intrinsic time measure-plasticity as a limit of the endochronic theory", *Arch. Mech.*, **32**, 171-191.
Watanabe, O. and Atluri, S.N. (1985), "A new endochronic approach to computational elasto-plasticity: An example of cyclically loaded cracked plate", *J. Appl. Mech.*, **25**, 857-864.
Watanabe, O. and Atluri, S.N. (1986), "Constitutive modeling of cyclic plasticity and creep, using an internal time concept", *Int. J. Plasticity*, **2**(2), 107-134.
Wu, H.C., Lu, J.K. and Pan, W.F. (1995), "Endochronic equations for finite plastic deformation and application to metal tube under torsion", *Int. J. Solids Struct.*, **32**(8/9), 1079-1097.
Wu, H.C. and Ho, C.C. (1995), "Strain hardening of annealed 304 stainless steel by creep", *J. Engng. Mat. Tech.*, ASME, **117**, 260-267.
Wu, H.C., Wang, T.P., Pan, W.F. and Xu, Z.Y. (1990), "Cyclic stress-strain response of porous aluminum", *Int. J. Plasticity*, **6**, 207-230.
Yeh, M.K. and Kyriakides, S. (1986), "On the collapse of inelastic thick-walled tubes under external pressure", *J. Energy Res. Tech.*, ASME, **18**, 35-47.